arXiv:1606.03026v4 [hep-ph] 19 Jul 2016

Signal-background interference for a singlet spin-0 digluon resonance at the LHC

Stephen P. Martin

Department of Physics, Northern Illinois University, DeKalb IL 60115

Dijet mass distributions can be used to search for spin-0 resonances that couple to two gluons. I show that there is a substantial impact on such searches from the interference between the resonant signal and the continuum QCD background amplitudes. The signal dijet mass distribution is qualitatively modified by this interference, compared to the naive expectation from considering only the pure resonant contribution, even if the total width of the resonance is minimal and very small compared to the experimental dijet mass resolution. The impact becomes more drastic as the total width of the resonance increases. These considerations are illustrated using examples relevant to the 750 GeV diphoton excess recently observed at the LHC.

Contents

I. Introduction 1

II. Signal-background interference at parton level 3

III. Numerical results for $\sqrt{s} = 8$ TeV 6

IV. Numerical results for $\sqrt{s} = 13$ TeV 10

V. Outlook 12

References 13

I. INTRODUCTION

In their LHC Run 2 data sets at $\sqrt{s} = 13$ TeV, the ATLAS and CMS experiments have each observed [1, 2] a local excess of events in $pp \to \gamma\gamma$, peaked at invariant mass near 750 GeV. This excess cannot be explained within the Standard Model except by statistical fluctuation, and it has therefore provoked a very high momentum (massive and fast) literature seeking to interpret it. A recent review containing references to this literature can be found in ref. [3]. One obvious class of candidate models is reminiscent of the Standard

Model Higgs boson, and consists of a new gauge-singlet spin-0 particle, called X here, of mass $M \approx 750$ GeV, which couples by non-renormalizable dimension-5 operators to gluon pairs and to photon pairs, providing the production mode $gg \to X$ and the decay $X \to \gamma\gamma$.

That class of models necessarily also predicts a dijet signal from $X \to gg$. The QCD background for the process $pp \to jj$ is very large, and the effects of QCD radiation, hadronization, and detector resolution are considerably less favorable than for the diphoton signal. However, it is clear that this is a way to limit (or explore) the coupling parameter space of these models. When the Xgg coupling is too large, the model parameter point can in principle be ruled out by checking that the dijet invariant mass spectrum is smooth and consistent with the predictions of the Standard Model. In this paper, I will use X to refer more generally to a singlet spin-0 (scalar or pseudoscalar) digluon resonance, without necessarily requiring it to be relevant to the 750 GeV diphoton excess.

The study of dijet mass distributions at hadron colliders has a long history, with developments before 2012 reviewed in ref. [4]. Because of high background rates, using the LHC to set limits near dijet mass 750 GeV is somewhat more problematic than at higher masses, and requires special handling to reduce data size and/or inefficiency due to trigger prescaling of the data sets. At this writing, the most recent limits on 750 GeV dijet resonances (not specialized to gauge-singlet, nor to spin 0, nor to decays into gluon pairs rather than quark-antiquark or quark-gluon) have been given by ATLAS in ref. [5] and by CMS in ref. [6]. The CMS limit, which uses a technique called data scouting to evade the trigger pre-scaling limitations, and wide jets to improve the dijet mass resolution of the signal (as in a previous CMS search [7]), has been variously interpreted (see for example [8–12]) by theorists interested in the 750 GeV diphoton excess to imply an upper limit of from 1 to 4 pb on the cross-section at $\sqrt{s} = 8$ TeV for resonant production of X with decays to digluons.

The purpose of the present paper is to point out that when interpreting such dijet searches it is important to take into account the interference between the resonant signal $gg \to X \to gg$ process and the continuum QCD background amplitude $gg \to gg$. In general, the impact of signal/background interference is greatest when the continuum QCD amplitudes are much larger than the amplitudes for the resonant production, as is the case here. An earlier study of QCD continuum-resonance interference for the dijet signal in the case of a spin-1 resonance was performed in ref. [13].

In the analogous case of $gg \to h \to \gamma\gamma$ involving a Standard Model Higgs boson, signal-background interference has been studied in refs. [14–21]. The interference effect on the total cross-section at the leading order (LO) was found to be very small in [14], but beyond the leading order it was shown [15] to suppress the diphoton cross-section by a few per cent for $M_h = 125$ GeV. Apart from this effect on the total cross-section, it was noted in ref. [16] that the interference causes a shift of the invariant mass position of the Higgs diphoton peak to slightly lower mass, compared to the real part of the Higgs pole mass. It was subsequently found that in events with emission of a hard jet [17, 18] the shift is much smaller and goes in the opposite direction. Ref. [19] provided a complete next-to-leading order (NLO) calculation, and found that the total mass shift is expected to be about 60 to 70 MeV, assuming Standard Model couplings. Ref. [19] also pointed out that the diphoton

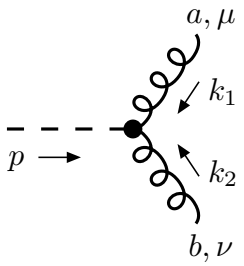

$$-i\frac{2c_g}{M^2}\delta^{ab}(k_1\cdot k_2\,\eta^{\mu\nu} - k_2^\mu k_1^\nu) \qquad \text{(scalar)}$$

$$-i\frac{2c_g}{M^2}\delta^{ab}\epsilon^{\mu\nu\rho\sigma}k_{1\rho}k_{2\sigma} \qquad \text{(pseudoscalar)}$$

FIG. 2.1: The Feynman rule for the effective Xgg coupling, with $p^\mu = -k_1^\mu - k_2^\mu$, for X = scalar (top) and pseudoscalar (bottom). Here c_g is a momentum-dependent form factor coupling that is approximately constant if the interaction comes from integrating out loops of heavier particles.

mass peak shift can, in principle, be used to place a model-independent bound† on the width of the Higgs boson in the case that it is not Standard Model. The mass peak shift for events with two additional jets has also been found to be small [20], so that this class of events can provide another reference point (along with the ZZ^* 4-lepton distribution) against which the shift can be measured. For the case of a 750 GeV resonance, the signal/background interference in the diphoton channel has been studied in refs. [34, 35] in the spin-0 case and ref. [36] in the spin-2 case, and in the $t\bar{t}$ final state in ref. [35]. Earlier studies of signal-background interference in $t\bar{t}$ production in various other new physics contexts can be found, for example, in refs. [37]. Resonance-continuum interference at hadron colliders has also been studied for W' and Z' production; see refs. [38] and refs. [39] respectively for examples.

As we will see below, the signal-background interference effect in $gg \to X \to gg$ is not negligible. The interference can produce a striking qualitative as well as quantitative difference compared to the naive Breit-Wigner s-channel estimate, the more so if the total width of X is larger than the partial width into two gluons, but the effect is substantial even if X decays mostly into two gluons. This should be taken into account to correctly set limits (or establish a non-Standard Model contribution) using dijet mass distributions.

II. SIGNAL-BACKGROUND INTERFERENCE AT PARTON LEVEL

The singlet spin-0 resonance X is assumed to couple to two gluons with an effective field theory Feynman rule shown in Figure 2.1, with different expressions for the scalar and pseudoscalar cases. In this paper, the gluons will always be on-shell and transverse. With this restriction, the momentum dependence of the effective form factor coupling c_g can only be through p^2, the invariant mass of the digluon pair. If this interaction arises from loops of heavier particles, as in the case of the Standard Model Higgs boson coupling induced by a top-quark loop, then in both the scalar and pseudoscalar cases for X the coupling c_g will be

† The far off-shell behavior of $pp \to h \to VV$ [22] can also be [23–27], and has been [28–30], used to bound the Higgs width, but in a somewhat more model-dependent way [31–33].

approximately constant. Because the Feynman rule scales with p^2, it is convenient to define

$$C_g(p^2) = \frac{p^2}{M^2} c_g. \tag{2.1}$$

For simplicity, the form eq. (2.1) with constant c_g will be assumed in the following, although more complicated form factors could ensue if the particles inducing c_g are not much heavier than X. This coupling can then be related to the LO digluon partial width of X, in both the scalar and pseudoscalar cases, by

$$\Gamma_{gg} = |c_g|^2 / 2\pi M. \tag{2.2}$$

The particle X has a total width Γ, which may include other decay modes, including $\gamma\gamma$.

At leading order, the digluon production cross-section can be written as (including a factor of 1/2 for identical final-state gluons):

$$\frac{d\sigma_{pp\to gg}}{d(\sqrt{\hat{s}})} \;=\; \frac{\sqrt{\hat{s}}}{s} \int_{\ln\sqrt{\tau}}^{-\ln\sqrt{\tau}} dy\, g(\sqrt{\tau}e^{y}) g(\sqrt{\tau}e^{-y}) \int_{-1}^{1} dz\, \Theta(\hat{s}, y, z)\, \frac{d\hat{\sigma}}{dz}. \tag{2.3}$$

Here $\sqrt{s}$ is the total energy of the pp collisions at the LHC, and $\sqrt{\hat{s}}$ is the total partonic center-of-momentum energy, equal to the invariant mass of the gluon pairs in both the initial and final states. Also, $\tau = \hat{s}/s$, and $g(x)$ is the gluon parton distribution function, y is the longitudinal rapidity of the digluon center-of-momentum frame, and z is the cosine of the gluon scattering angle with respect to the proton beams. The factor $\Theta(\hat{s}, y, z)$ represents the effects of kinematic cuts.

The naive partonic LO differential cross-section from only the s-channel resonant amplitude is, in both the scalar and pseudoscalar cases,

$$\frac{d\hat{\sigma}_s}{dz} \;=\; \frac{|C_g(\hat{s})|^4}{32\pi \hat{s} D(\hat{s})}, \tag{2.4}$$

where

$$D(\hat{s}) \;=\; (\hat{s} - M^2)^2 + \Gamma^2 M^2. \tag{2.5}$$

In the narrow-width approximation, one takes

$$1/D(\hat{s}) \;=\; \pi\delta(\hat{s} - M^2)/\Gamma M, \tag{2.6}$$

so that after integrating over $\sqrt{\hat{s}}$ using the MSTW 2008 NLO [40] parton distribution func-

tion for the gluon with factorization scale $\mu_F = M = 750$ GeV, one obtains a LO cross-section

$$\sigma(pp \to X \to gg) \approx \frac{\Gamma_{gg}^2}{M\Gamma} \times \begin{cases} 1.06 \times 10^3 \text{ pb} & (\text{for } \sqrt{s} = 8 \text{ TeV}), \\ 4.92 \times 10^3 \text{ pb} & (\text{for } \sqrt{s} = 13 \text{ TeV}). \end{cases} \tag{2.7}$$

However, the above is based on the narrow-width approximation without interference effects, which is fictional. In reality, the complete LO partonic differential cross-section involving X, in excess of the pure QCD background but including interference with it, contains other contributions:

$$\begin{aligned} \frac{d\hat{\sigma}}{dz} &= \frac{d\hat{\sigma}_s}{dz} + \frac{d\hat{\sigma}_t}{dz} + \frac{d\hat{\sigma}_u}{dz} + \frac{d\hat{\sigma}_{s,t}}{dz} + \frac{d\hat{\sigma}_{s,u}}{dz} + \frac{d\hat{\sigma}_{t,u}}{dz} \\ &\quad + \frac{d\hat{\sigma}_{s,\text{QCD}}}{dz} + \frac{d\hat{\sigma}_{t,\text{QCD}}}{dz} + \frac{d\hat{\sigma}_{u,\text{QCD}}}{dz}. \end{aligned} \tag{2.8}$$

The most important individual contribution in addition to eq. (2.4) is the interference of the s-channel X exchange diagram with the pure QCD amplitude. In both the scalar and pseudoscalar cases, I find:

$$\frac{d\hat{\sigma}_{s,\text{QCD}}}{dz} = -\frac{3\alpha_S}{8\hat{s}D(\hat{s})(1-z^2)} \left\{ \text{Re}[C_g(\hat{s})^2](\hat{s} - M^2) + \text{Im}[C_g(\hat{s})^2]M\Gamma \right\}. \tag{2.9}$$

The contribution of eq. (2.9) nearly vanishes for $\hat{s} = M^2$, but has maximal excursions from 0 near $\sqrt{\hat{s}} = M \pm \Gamma/2$ that can be numerically larger than the pure resonant contribution of eq. (2.4), especially when Γ/Γ_{gg} is large. It has a characteristic peak-dip structure, which partially washes out due to detector resolution and QCD radiation effects; this cancellation is less complete when Γ is comparable to the effective dijet mass resolution. More importantly, far from the resonance mass M, the Breit-Wigner tails are enhanced by the numerator factor of $\hat{s} - M^2$ in the interference term of eq. (2.9). There is a suppression (enhancement) of the magnitude of the lower (upper) tail from the $\hat{s}^2$ factor following from the momentum dependence of the C_g coupling, but this is counteracted by the falling $\hat{s}$ dependence of the gluon-gluon luminosity function.

The remaining contributions from diagrams with t-channel and u-channel exchanges of X, and their interferences with the resonant s-channel and QCD diagrams, are numerically smaller. Here the scalar and pseudoscalar cases part company. If X is a scalar:

$$\frac{d\hat{\sigma}_t}{dz} + \frac{d\hat{\sigma}_u}{dz} = \frac{(1+z^2)^2}{128\pi\hat{s}} \left[\frac{|C_g(\hat{t})|^4}{(\hat{t} - M^2)^2} + \frac{|C_g(\hat{u})|^4}{(\hat{u} - M^2)^2} \right], \tag{2.10}$$

$$\frac{d\hat{\sigma}_{t,u}}{dz} = \frac{\text{Re}[C_g(\hat{t})^2\, C_g(\hat{u})^{*2}](1+z^4)}{512\pi\hat{s}(\hat{t} - M^2)(\hat{u} - M^2)}, \tag{2.11}$$

$$\frac{d\hat{\sigma}_{s,t}}{dz} = \frac{\left\{ \text{Re}[C_g(\hat{s})^2\, C_g(\hat{t})^{*2}](\hat{s} - M^2) + \text{Im}[C_g(\hat{s})^2\, C_g(\hat{t})^{*2}]\Gamma M \right\}(1+z^2)}{512\pi\hat{s}D(\hat{s})(\hat{t} - M^2)}, \tag{2.12}$$

$$\frac{d\hat{\sigma}_{s,u}}{dz} = \frac{\{\mathrm{Re}[C_g(\hat{s})^2\, C_g(\hat{u})^{*2}](\hat{s}-M^2) + \mathrm{Im}[C_g(\hat{s})^2\, C_g(\hat{u})^{*2}]\Gamma M\}\,(1+z^2)}{512\pi\hat{s}D(\hat{s})(\hat{u}-M^2)}, \quad (2.13)$$

$$\frac{d\hat{\sigma}_{t,\mathrm{QCD}}}{dz} = \frac{3\alpha_S \mathrm{Re}[C_g(\hat{t})^2](3+4z+8z^2+z^4)}{128\hat{s}(\hat{t}-M^2)(1+z)}, \quad (2.14)$$

$$\frac{d\hat{\sigma}_{u,\mathrm{QCD}}}{dz} = \frac{3\alpha_S \mathrm{Re}[C_g(\hat{u})^2](3-4z+8z^2+z^4)}{128\hat{s}(\hat{u}-M^2)(1-z)}, \quad (2.15)$$

while if X is a pseudoscalar, one has instead:

$$\frac{d\hat{\sigma}_t}{dz} + \frac{d\hat{\sigma}_u}{dz} = \frac{1}{32\pi\hat{s}}\left[\frac{|C_g(\hat{t})|^4}{(\hat{t}-M^2)^2} + \frac{|C_g(\hat{u})|^4}{(\hat{u}-M^2)^2}\right], \quad (2.16)$$

$$\frac{d\hat{\sigma}_{t,u}}{dz} = \frac{\mathrm{Re}[C_g(\hat{t})^2\, C_g(\hat{u})^{*2}]}{256\pi\hat{s}(\hat{t}-M^2)(\hat{u}-M^2)}, \quad (2.17)$$

$$\frac{d\hat{\sigma}_{s,t}}{dz} = \frac{\mathrm{Re}[C_g(\hat{s})^2\, C_g(\hat{t})^{*2}](\hat{s}-M^2) + \mathrm{Im}[C_g(\hat{s})^2\, C_g(\hat{t})^{*2}]\Gamma M}{256\pi\hat{s}D(\hat{s})(\hat{t}-M^2)}, \quad (2.18)$$

$$\frac{d\hat{\sigma}_{s,u}}{dz} = \frac{\mathrm{Re}[C_g(\hat{s})^2\, C_g(\hat{u})^{*2}](\hat{s}-M^2) + \mathrm{Im}[C_g(\hat{s})^2\, C_g(\hat{u})^{*2}]\Gamma M}{256\pi\hat{s}D(\hat{s})(\hat{u}-M^2)}, \quad (2.19)$$

$$\frac{d\hat{\sigma}_{t,\mathrm{QCD}}}{dz} = \frac{3\alpha_S \mathrm{Re}[C_g(\hat{t})^2](1-z)^2}{64\hat{s}(\hat{t}-M^2)(1+z)}, \quad (2.20)$$

$$\frac{d\hat{\sigma}_{u,\mathrm{QCD}}}{dz} = \frac{3\alpha_S \mathrm{Re}[C_g(\hat{u})^2](1+z)^2}{64\hat{s}(\hat{u}-M^2)(1-z)}. \quad (2.21)$$

Above, I have neglected $i\Gamma M$ in the t-channel and u-channel propagators. Of these contributions involving t-channel and u-channel exchange, only the ones that involve interference with QCD [eqs. (2.14)-(2.15) or (2.20)-(2.21)] are numerically appreciable in the examples below, but all are included for completeness. The large and well-known continuum pure QCD contributions to the differential cross-section are not shown, and in practice are modeled by the experimental collaborations using a parameterized smoothly falling background. In the following, I will also assume that there is no absorptive part of the Xgg form factor, so that $C_g(p^2)$ is always real. Below, I will only present numerical results for the scalar case, because it turns out that the numerical differences between the scalar and the pseudoscalar cases are extremely small.

III. NUMERICAL RESULTS FOR $\sqrt{s} = 8$ TEV

In this section, I will numerically illustrate the impact of the interference effects for the LHC runs with $\sqrt{s} = 8$ TeV. In order to be approximately relevant to the boundary of the region that has sometimes been taken to be excluded by the CMS result [6], I will choose benchmarks that in the naive narrow-width approximation would yield $\sigma(pp \to X \to jj) \approx 2.5$ pb at $\sqrt{s} = 8$ TeV. Using eq. (2.7) and including a K factor of 1.5, this implies $\Gamma_{gg}^2/\Gamma \approx 0.0016M$. Therefore, I will take as one benchmark scenario the case that this is

saturated, with $\Gamma_{\gamma\gamma}$ and all other partial widths much smaller:

$$\Gamma_{gg} = \Gamma = 0.0016M, \tag{3.1}$$

which implies $c_g = 75$ GeV. If instead X also has significant decay widths into other states, so that the total width Γ is larger than Γ_{gg}, then obtaining 2.5 pb for the narrow-width prediction cross-section requires larger Γ_{gg}, and therefore larger c_g, according to eq. (2.2). There are significant constraints on partial widths into other Standard Model 2-body final states, including X decaying to invisible particles (see for example [9, 12]). However, if X can decay into more nondescript (but not invisible) final states, for example collections of soft jets, then these constraints may not apply, and Γ can be larger than Γ_{gg}. I will therefore consider below two other benchmark cases:

$$\Gamma_{gg} = 0.004M, \qquad \Gamma = 0.01M, \tag{3.2}$$

and

$$\Gamma_{gg} = 0.01M, \qquad \Gamma = 0.06M. \tag{3.3}$$

The last case is of interest because ATLAS has found [1] that the data may prefer a width to mass ratio of order 6%. One could even consider larger widths Γ as being compatible with the excesses observed by both ATLAS and CMS.

For purposes of illustration, I apply parton-level cuts $p_T > 40$ GeV, and $|\eta| < 2.5$ on the gluons following ref. [6]. The resulting digluon invariant mass distributions for $pp \to gg$, from the formulas in the preceding section, are shown in Figure 3.1 as a function of $m = \sqrt{\hat{s}}$. The thinner (red) line shows the fictional result with only the s-channel resonance diagram $gg \to X \to gg$ [from eq. (2.4)] included, while the thicker (blue) line is the full result including the t-channel and u-channel exchange of X and their interferences with the continuum QCD $gg \to gg$ diagrams, from eqs. (2.4), (2.9), and (2.10)-(2.15). The peak of the full distribution is somewhat larger in magnitude and slightly lower in mass than the naive resonant-only approximation, but the extensive positive and negative tails will be of greater importance after resolution effects, as shown below. Note that $d\sigma/dm$ is negative where the interference dominates and is destructive, because the pure continuum QCD background contribution, not shown, renders the total positive. (No K factors are included in these plots.)

Similarly, Figure 3.2 shows the parton-level digluon mass distributions for the cases with larger widths given in eqs. (3.2) and (3.3). These figures show that with $\Gamma > \Gamma_{gg}$, the interference effect is much larger than the naive pure resonance contribution, with fatter positive and negative tails below and above M.

In order to approximately model the detector responses for the dijet invariant mass distributions, below I will smear the final state digluon invariant masses by convolution with a double-sided crystal ball function [41] with a cutoff at large masses, i.e., a Gaussian core smoothly matched to power-law tails on each side. For a given input digluon invariant mass m_{gg}, this distribution function for the observed dijet invariant mass m is approximated

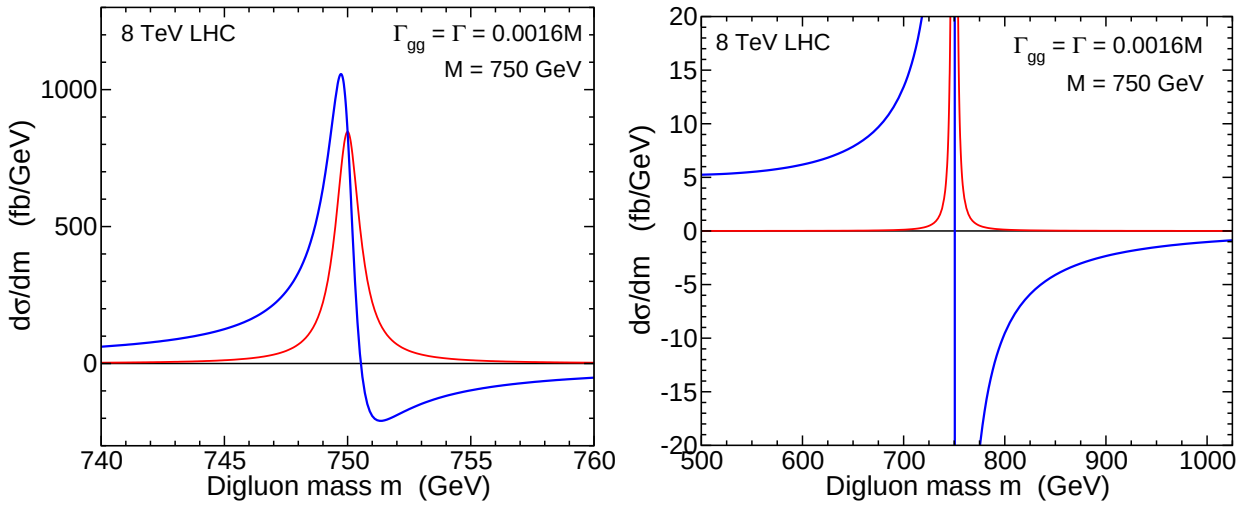

FIG. 3.1: The digluon invariant mass distribution for $pp \to gg$ at leading order, for the case $\Gamma_{gg} = \Gamma_{\rm tot} = 0.0016M$. The thinner (red) lines show the fictional result with only the s-channel resonance diagram $gg \to X \to gg$ included, while the thicker (blue) lines show the full result from eqs. (2.4), (2.9), and (2.10)-(2.15) including interferences with the continuum QCD $gg \to gg$ amplitude. The two panels show the same data but with different scales on the axes.

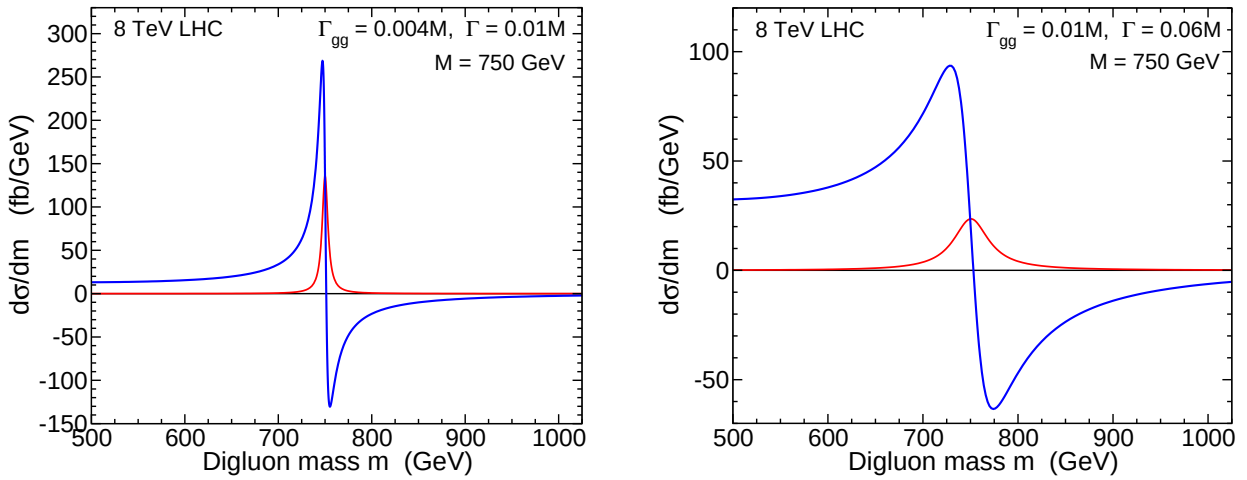

FIG. 3.2: The digluon invariant mass distribution for $pp \to gg$ at leading order, for the cases $\Gamma_{gg} = 0.004M$ and $\Gamma_{\rm tot} = 0.01M$ (left panel) and $\Gamma_{gg} = 0.01M$ and $\Gamma_{\rm tot} = 0.06M$ (right panel). The thinner (red) lines show the fictional results with only the s-channel resonance diagram $gg \to X \to gg$ included, while the thicker (blue) lines show the full results from eqs. (2.4), (2.9), and (2.10)-(2.15) including interference with the continuum QCD $gg \to gg$ amplitude.

by the form:

$$f(m, m_{gg}) \;=\; N \begin{cases} (A_L + B_L m)^{-n_L} & \text{for } (m-\overline{m})/\sigma \le -\alpha_L, \\ \exp[-(m-\overline{m})^2/2\sigma^2] & \text{for } -\alpha_L \le (m-\overline{m})/\sigma \le \alpha_H, \\ (1-m/m_{\rm max})^{\nu}(A_H + B_H m)^{-n_H} & \text{for } (m-\overline{m})/\sigma \ge \alpha_H. \end{cases} \quad (3.4)$$

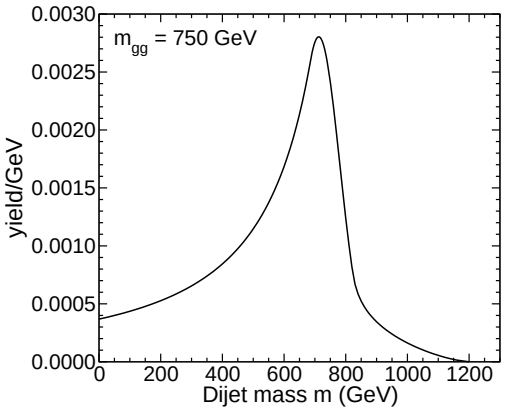

FIG. 3.3: The assumed normalized detector response dijet mass distribution, from eq. (3.4), for the example case of a gluon pair with invariant mass $m_{gg} = 750$ GeV.

Here, the width in the Gaussian core of the distribution is taken to be $\sigma/m_{gg} = 2.09/\sqrt{m_{gg}} + 0.015$ as obtained in the CMS wide jet analyses [6, 7]. I also use $\overline{m} = 0.95 m_{gg}$, $m_{\rm max} = 1.6 m_{\rm gg}$, $n_L = 1.5$, $\alpha_L = 0.4$, $n_H = 0.25$, $\alpha_H = 1.6$, and $\nu = 1.4$, estimated to roughly match Figure 2 in ref. [6] when $m_{gg} = 900$ GeV. The constants A_L, B_L, A_H, B_H are then uniquely determined in terms of the other parameters by the continuity of $f(m, m_{gg})$ and its first derivative with respect to m, and the normalization constant N is fixed by the requirement $\int_0^{m_{\rm max}} f(m, m_{gg})\, dm = 1$. As an illustration, the function $f(m, m_{gg})$ is shown in Figure 3.3 for the example case $m_{gg} = 750$ GeV.

After smearing by convolution with the parton-level results using eq. (3.4), one obtains the distributions shown in Figure 3.4, for the three benchmark cases described above. The case with $\Gamma_{gg} = \Gamma = 0.0016M$ has the smallest effect from the interference with QCD, but even in this case one sees that the resulting dijet mass distribution is very different from the naive expectation obtained by including only the s-channel X exchange amplitude. The maximum excursion from 0 is about 50% larger than the naive expectation, and is more of a plateau rather than a peak. In the resonance region $m \approx M$, the full distribution falls rapidly until reaching a shallow but long negative tail for $m > 800$ GeV. It is not immediately clear how this will affect the setting of limits, because it depends on how the QCD background is parameterized in the data analysis. In particular, in the case that the signal is present, the positive tail for $m < 700$ GeV might be absorbed into the background fit, leading to a smaller peak at lower m and an apparent dip for $m > 700$ GeV, rather than a pure peak.

For the larger total width cases shown, with $\Gamma = 0.01M$ and $0.06M$, the off-resonance positive and negative tails from the $\hat{s} - M^2$ numerator factor in eq. (2.9) become much more pronounced, as they are enhanced by a larger c_g^2 factor. In these cases, the dip would be impossible to miss if the effect of X is visible at all, regardless of the method used to model the background. It is clear that the interference effect is crucial in interpreting the dijet mass distribution in order to set search limits on a digluon resonance, as the naive pure resonance behavior is completely different from the full result, both qualitatively and quantitatively.

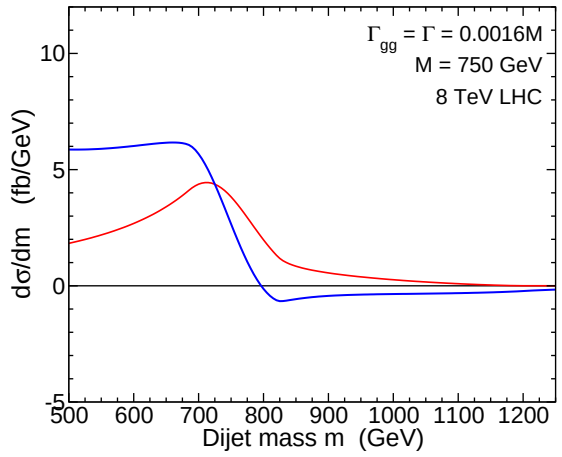

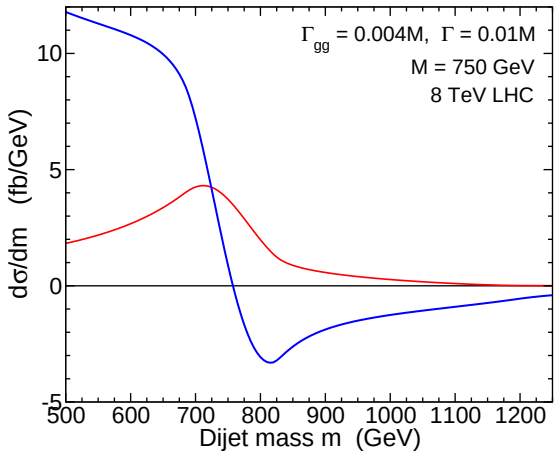

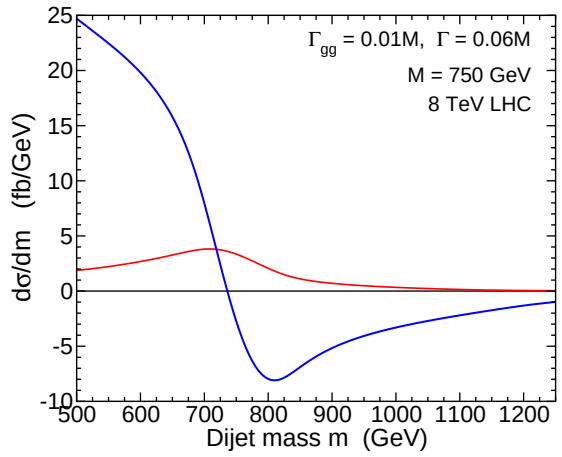

FIG. 3.4: Dijet invariant mass distributions for the benchmark examples of eqs. (3.1)-(3.3), at $\sqrt{s} = 8$ TeV, obtained by smearing the digluon mass distributions using convolution by the function in eq. (3.4). The thinner (red) lines show the fictional results with only the s-channel resonance diagram $gg \to X \to gg$ included, while the thicker (blue) lines show the full results including interferences with the continuum QCD $gg \to gg$ amplitudes and the t- and u-channel exchanges of X.

IV. NUMERICAL RESULTS FOR $\sqrt{s} = 13$ TEV

At this writing, the LHC is colliding protons with $\sqrt{s} = 13$ TeV, adding to the existing data sets at that energy which gave rise to the 750 GeV diphoton excess. Whether or not that excess is confirmed, it will be important to look for dijet anomalies as part of a robust program of searches for physics beyond the Standard Model. In this section, I consider a few benchmark cases for a singlet spin-0 resonance at this higher energy.

From the formulas in section II, it becomes apparent that the relative shapes of the full and naive dijet mass distributions at leading order have only a weak dependence on $\sqrt{s}$. This is because all of the contributions to $d\sigma/dz$ are multiplied by the same gluon-gluon luminosity function, for a given $\sqrt{s}$. There is a dependence on kinematic cuts, which produce relatively minor differences in shape. The main dependences of the shapes of the distributions come instead from the total width Γ and the coupling strength parameterized by Γ_{gg} according to eq. (2.2). Therefore, as benchmarks I choose four cases picked so that in each case the naive narrow-width approximation would give a total cross-section of about 3 pb from eq. (2.7) at $\sqrt{s} = 13$ TeV after including a K factor of 1.5. Results obtained by scaling Γ and Γ_{gg} by a common factor should have different magnitudes but roughly the

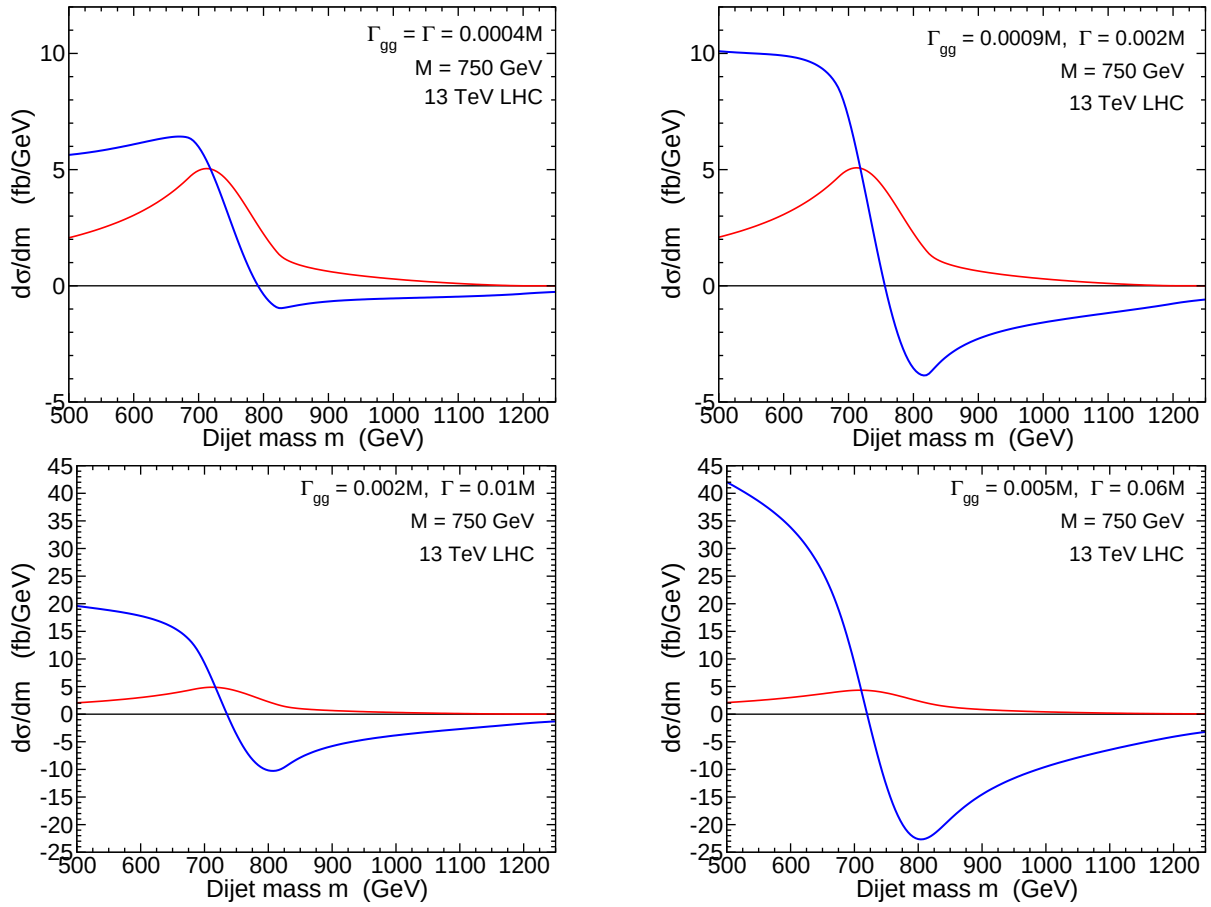
Γgg = Γ = 0.0004M
M = 750 GeV
13 TeV LHC
Γgg = 0.0009M, Γ = 0.002M
M = 750 GeV
13 TeV LHC
Γgg = 0.002M, Γ = 0.01M
M = 750 GeV
13 TeV LHC
Γgg = 0.005M, Γ = 0.06M
M = 750 GeV
13 TeV LHC
dσ/dm (fb/GeV)
Dijet mass m (GeV)

FIG. 4.1: Dijet invariant mass distributions for the benchmark examples of eqs. (4.1)-(4.4), with $\sqrt{s} = 13$ TeV, obtained by smearing the digluon mass distributions using convolution by the function in eq. (3.4). The thinner (red) lines show the fictional results with only the s-channel resonance diagram $gg \to X \to gg$ included, while the thicker (blue) lines show the full results including interferences with the continuum QCD $gg \to gg$ amplitudes and the t- and u-channel exchanges of X.

same shapes. The four chosen benchmark cases for $\sqrt{s} = 13$ TeV are:

$$\Gamma_{gg} = \Gamma = 0.0004M, \tag{4.1}$$
$$\Gamma_{gg} = 0.0009M, \qquad \Gamma = 0.002M, \tag{4.2}$$
$$\Gamma_{gg} = 0.002M, \qquad \Gamma = 0.01M, \tag{4.3}$$
$$\Gamma_{gg} = 0.005M, \qquad \Gamma = 0.06M. \tag{4.4}$$

The first case eq. (4.1) is the minimal width for the given target narrow-width approximation cross-section, while the last eq. (4.4) is included because of the present ATLAS preference for a large width when the model is intended to explain the 750 GeV diphoton excess.

The dijet mass distributions obtained after smearing by convolution with the response function in eq. (3.4) are shown in Figure 4.1. As promised, the minimal width case has a strong resemblance in shapes to the minimal width benchmark case at $\sqrt{s} = 8$ TeV with

$\Gamma = \Gamma_{gg}$ (compare the first panel of Figure 3.4). This represents the minimal impact of the QCD interference contributions compared to the naive s-channel X exchange contribution. As the ratio Γ/Γ_{gg} increases, the positive and negative tails from the QCD interference become more dominant.

V. OUTLOOK

In this paper, I have argued that the effects of interference with the QCD continuum background must be included when searching for digluon resonances at the LHC. The interference effects can overwhelm the naive pure resonance contribution even if the width of the resonance is much smaller than the dijet mass resolution. Although the numerical examples here were confined to the case of $M = 750$ GeV, I have checked that the results are quite similar for larger masses.

Only the leading order effects have been included here, so the results obtained only demonstrate the importance and the general size of the effect. It is clear that for a more realistic numerical estimate, it will be necessary to include at least NLO corrections with virtual 1-loop and real emission of an extra jet. In this regard, note that the real emission contributions with an extra jet could well have a quite different structure of interference with the QCD background, as they come in part from quark-gluon and quark-antiquark scattering, with completely different initial and final states. In the somewhat analogous case of $gg \to h \to \gamma\gamma$ in the Standard Model, recall that emission of one or two additional jets (with e.g. $p_T > 30$ GeV) results in a much smaller shift [17–20] in the Higgs diphoton peak compared to the LO shift [16]. It remains to be seen how such NLO effects behave in the present situation. It would also be interesting to evaluate the impact of resonance-continuum interference on dijet resonances with other spin and color quantum number assignments, including for example a spin-2 singlet resonance, or a resonance that decays to $q\overline{q}$.

I have not attempted a full Monte Carlo simulation of the detector responses, which could not be as accurate as results from the ATLAS and CMS detector collaborations themselves. In the search for a spin-0 digluon resonance, greater sensitivity can probably be obtained by enforcing a harder cut on the leading two jet transverse momenta in addition to the generic dijet mass spectrum requirements, because the LO pure resonance signal (before cuts) is isotropic in the center-of-momentum frame, while the LO pure QCD background is forward-backward peaked, with $1/(1 \pm z)^2$ singularities for scattering near the beam axis where $z = \mp 1$. Note that the LO X-QCD interference term is intermediate between these, with $1/(1 \pm z)$ behavior as seen in eq. (2.9). A stringent cut on the p_T for the second leading jet would therefore seem to be appropriate to formally maximize significance for the signal (including interference) for a singlet spin-0 resonance over the pure QCD background at leading order, but this should be re-evaluated for optimization after including NLO and QCD radiation and detector resolution effects, which can have a strong impact on the jet p_T distributions. If a dijet mass anomaly is detected or suspected in future data, the p_T dependence will depend on the inclusion of interference effects, and could also be used to probe or limit its possible origin from a resonance.

Acknowledgments: This work was supported in part by the National Science Foundation grant number PHY-1417028.

[1] ATLAS collaboration, "Search for resonances decaying to photon pairs in 3.2 fb^{-1} of pp collisions at $\sqrt{s} = 13$ TeV with the ATLAS detector," ATLAS-CONF-2015-081. "Search for resonances in diphoton events with the ATLAS detector at $\sqrt{s} = 13$ TeV," ATLAS-CONF-2016-018.

[2] CMS collaboration, "Search for new physics in high mass diphoton events in proton-proton collisions at 13TeV," CMS-PAS-EXO-15-004. "Search for new physics in high mass diphoton events in 3.3 fb^{-1} of proton-proton collisions at $\sqrt{s} = 13$ TeV and combined interpretation of searches at 8 TeV and 13 TeV," CMS-PAS-EXO-16-018.

[3] A. Strumia, "Interpreting the 750 GeV digamma excess: a review," arXiv:1605.09401 [hep-ph].

[4] R. M. Harris and K. Kousouris, "Searches for Dijet Resonances at Hadron Colliders," Int. J. Mod. Phys. A **26**, 5005 (2011) [arXiv:1110.5302 [hep-ex]].

[5] G. Aad *et al.* [ATLAS Collaboration], "Search for new phenomena in the dijet mass distribution using $p - p$ collision data at $\sqrt{s} = 8$ TeV with the ATLAS detector," Phys. Rev. D **91**, no. 5, 052007 (2015) [arXiv:1407.1376 [hep-ex]].

[6] V. Khachatryan *et al.* [CMS Collaboration], "Search for narrow resonances in dijet final states at sqrt(s)=8 TeV with the novel CMS technique of data scouting," arXiv:1604.08907 [hep-ex].

[7] S. Chatrchyan *et al.* [CMS Collaboration], "Search for Resonances in the Dijet Mass Spectrum from 7 TeV pp Collisions at CMS," Phys. Lett. B **704**, 123 (2011) [arXiv:1107.4771 [hep-ex]].

[8] S. Knapen, T. Melia, M. Papucci and K. Zurek, "Rays of light from the LHC," Phys. Rev. D **93**, no. 7, 075020 (2016) [arXiv:1512.04928 [hep-ph]].

[9] R. Franceschini, G. F. Giudice, J. F. Kamenik, M. McCullough, A. Pomarol, R. Rattazzi, M. Redi, F. Riva, A. Strumia and R. Torre, "What is the $\gamma\gamma$ resonance at 750 GeV?," JHEP **1603**, 144 (2016) [arXiv:1512.04933 [hep-ph]].

[10] R. S. Gupta, S. Jäger, Y. Kats, G. Perez and E. Stamou, "Interpreting a 750 GeV Diphoton Resonance," arXiv:1512.05332 [hep-ph].

[11] A. Falkowski, O. Slone and T. Volansky, "Phenomenology of a 750 GeV Singlet," JHEP **1602**, 152 (2016) [arXiv:1512.05777 [hep-ph]].

[12] R. Franceschini, G. F. Giudice, J. F. Kamenik, M. McCullough, F. Riva, A. Strumia and R. Torre, "Digamma, what next?," arXiv:1604.06446 [hep-ph].

[13] D. Choudhury, R. M. Godbole and P. Saha, "Dijet resonances, widths and all that," JHEP **1201**, 155 (2012) [arXiv:1111.1054 [hep-ph]].

[14] D. A. Dicus and S. S. D. Willenbrock, "Photon Pair Production and the Intermediate Mass Higgs Boson," Phys. Rev. D **37**, 1801 (1988).

[15] L. J. Dixon and M. S. Siu, "Resonance continuum interference in the diphoton Higgs signal at the LHC," Phys. Rev. Lett. **90**, 252001 (2003) [hep-ph/0302233].

[16] S. P. Martin, "Shift in the LHC Higgs diphoton mass peak from interference with background," Phys. Rev. D **86**, 073016 (2012) [arXiv:1208.1533 [hep-ph]].

[17] D. de Florian, N. Fidanza, R. J. Hernández-Pinto, J. Mazzitelli, Y. Rotstein Habarnau and G. F. R. Sborlini, "A complete $O(\alpha_S^2)$ calculation of the signal-background interference for the Higgs diphoton decay channel," Eur. Phys. J. C **73**, no. 4, 2387 (2013) [arXiv:1303.1397].

[18] S. P. Martin, "Interference of Higgs diphoton signal and background in production with a jet at the LHC," Phys. Rev. D **88**, no. 1, 013004 (2013) [arXiv:1303.3342 [hep-ph]].

[19] L. J. Dixon and Y. Li, "Bounding the Higgs Boson Width Through Interferometry," Phys. Rev. Lett. **111**, 111802 (2013) [arXiv:1305.3854 [hep-ph]].

[20] F. Coradeschi, D. de Florian, L. J. Dixon, N. Fidanza, S. Hche, H. Ita, Y. Li and J. Mazzitelli, "Interference effects in the $H(\to \gamma\gamma) + 2$ jets channel at the LHC," Phys. Rev. D **92**, no. 1, 013004 (2015) [arXiv:1504.05215 [hep-ph]].

[21] C. P. Becot, "Diphoton lineshape of the BEH boson using the ATLAS detector at the LHC : calibration, mass, width and interferences," CERN-THESIS-2015-193, LAL-15-303.

[22] N. Kauer and G. Passarino, "Inadequacy of zero-width approximation for a light Higgs boson signal," JHEP **1208**, 116 (2012) [arXiv:1206.4803 [hep-ph]].

[23] F. Caola and K. Melnikov, "Constraining the Higgs boson width with ZZ production at the LHC," Phys. Rev. D **88**, 054024 (2013) [arXiv:1307.4935 [hep-ph]].

[24] J. M. Campbell, R. K. Ellis and C. Williams, "Bounding the Higgs width at the LHC using full analytic results for $gg \to e^- e^+ \mu^- \mu^+$," JHEP **1404**, 060 (2014) [arXiv:1311.3589].

[25] J. M. Campbell, R. K. Ellis and C. Williams, "Bounding the Higgs width at the LHC: Com-

plementary results from $H \to WW$," Phys. Rev. D **89**, no. 5, 053011 (2014) [arXiv:1312.1628].
[26] J. M. Campbell, R. K. Ellis, E. Furlan and R. Röntsch, "Interference effects for Higgs boson mediated Z-pair plus jet production," Phys. Rev. D **90**, no. 9, 093008 (2014) [arXiv:1409.1897].
[27] J. M. Campbell and R. K. Ellis, "Higgs Constraints from Vector Boson Fusion and Scattering," JHEP **1504**, 030 (2015) [arXiv:1502.02990 [hep-ph]].
[28] V. Khachatryan *et al.* [CMS Collaboration], "Constraints on the Higgs boson width from off-shell production and decay to Z-boson pairs," Phys. Lett. B **736**, 64 (2014)
[29] G. Aad *et al.* [ATLAS Collaboration], "Constraints on the off-shell Higgs boson signal strength in the high-mass ZZ and WW final states with the ATLAS detector," Eur. Phys. J. C **75**, no. 7, 335 (2015) [arXiv:1503.01060 [hep-ex]].
[30] V. Khachatryan *et al.* [CMS Collaboration], "Search for Higgs boson off-shell production in proton-proton collisions at 7 and 8 TeV and derivation of constraints on its total decay width," arXiv:1605.02329 [hep-ex].
[31] C. Englert and M. Spannowsky, "Limitations and Opportunities of Off-Shell Coupling Measurements," Phys. Rev. D **90**, 053003 (2014) [arXiv:1405.0285 [hep-ph]].
[32] C. Englert, Y. Soreq and M. Spannowsky, "Off-Shell Higgs Coupling Measurements in BSM scenarios," JHEP **1505**, 145 (2015) [arXiv:1410.5440 [hep-ph]].
[33] H. E. Logan, "Hiding a Higgs width enhancement from off-shell $gg(\to h^*) \to ZZ$ measurements," Phys. Rev. D **92**, no. 7, 075038 (2015) [arXiv:1412.7577 [hep-ph]].
[34] S. Jung, Y. W. Yoon and J. Song, "Interference effect on a heavy Higgs resonance signal in the $\gamma\gamma$ and ZZ channels," Phys. Rev. D **93**, no. 5, 055035 (2016) doi:10.1103/PhysRevD.93.055035 [arXiv:1510.03450 [hep-ph]]. S. Jung, J. Song and Y. W. Yoon, "How Resonance-Continuum Interference Changes 750 GeV Diphoton Excess: Signal Enhancement and Peak Shift," JHEP **1605**, 009 (2016) [arXiv:1601.00006 [hep-ph]].
[35] A. Djouadi, J. Ellis and J. Quevillon, "Interference Effects in the Decays of 750 GeV States into $\gamma\gamma$ and $t\bar{t}$," arXiv:1605.00542 [hep-ph].
[36] M. Fabbrichesi, M. Pinamonti and A. Urbano, "Telling the spin of the di-photon resonance," arXiv:1604.06948 [hep-ph].
[37] D. Dicus, A. Stange and S. Willenbrock, "Higgs decay to top quarks at hadron colliders," Phys. Lett. B **333**, 126 (1994) [hep-ph/9404359]. D. Choudhury, R. M. Godbole, R. K. Singh and K. Wagh, "Top production at the Tevatron/LHC and nonstandard, strongly interacting spin one particles," Phys. Lett. B **657**, 69 (2007) [0705.1499 [hep-ph]]. A. Djouadi, G. Moreau and R. K. Singh, "Kaluza-Klein excitations of gauge bosons at the LHC," Nucl. Phys. B **797**, 1 (2008) [0706.4191 [hep-ph]]. R. Frederix and F. Maltoni, "Top pair invariant mass distribution: A Window on new physics," JHEP **0901**, 047 (2009) [0712.2355 [hep-ph]]. U. Haisch and S. Westhoff, "Massive Color-Octet Bosons: Bounds on Effects in Top-Quark Pair Production," JHEP **1108**, 088 (2011) [1106.0529 [hep-ph]]. N. Craig, F. D'Eramo, P. Draper, S. Thomas and H. Zhang, "The Hunt for the Rest of the Higgs Bosons," JHEP **1506**, 137 (2015) [1504.04630 [hep-ph]]. B. Hespel, F. Maltoni and E. Vryonidou, "Signal background interference effects in heavy scalar production and decay to a top-anti-top pair," 1606.04149 [hep-ph].
[38] E. Boos, V. Bunichev, L. Dudko and M. Perfilov, "Interference between W' and W in single-top quark production processes," Phys. Lett. B **655**, 245 (2007) [hep-ph/0610080]. T. G. Rizzo, "The Determination of the Helicity of W' Boson Couplings at the LHC," JHEP **0705**, 037 (2007) [arXiv:0704.0235 [hep-ph]]. A. Papaefstathiou and O. Latunde-Dada, "NLO production of W' bosons at hadron colliders using the MC@NLO and POWHEG methods," JHEP **0907**, 044 (2009) [arXiv:0901.3685]. E. Accomando, D. Becciolini, S. De Curtis, D. Dominici, L. Fedeli and C. Shepherd-Themistocleous, "Interference effects in heavy W'-boson searches at the LHC," Phys. Rev. D **85**, 115017 (2012) [arXiv:1110.0713 [hep-ph]]. L. Bian, D. Liu, J. Shu and Y. Zhang, "Interference Effect on Resonance Studies in Searches of Heavy Particles," Int. J. Mod. Phys. **31**, no. 14n15, 1650083 (2016) [arXiv:1509.02787].
[39] E. Accomando, D. Becciolini, A. Belyaev, S. Moretti and C. Shepherd-Themistocleous, "Z' at the LHC: Interference and Finite Width Effects in Drell-Yan," JHEP **1310**, 153 (2013) [arXiv:1304.6700 [hep-ph]]. E. Accomando, D. Barducci, S. De Curtis, J. Fiaschi, S. Moretti and C. H. Shepherd-Themistocleous, "Drell-Yan production of multi Z'-bosons at the LHC within Non-Universal ED and 4D Composite Higgs Models," arXiv:1602.05438 [hep-ph].
[40] A. D. Martin, W. J. Stirling, R. S. Thorne and G. Watt, "Parton distributions for the LHC," Eur. Phys. J. C **63**, 189 (2009) [arXiv:0901.0002 [hep-ph]].
[41] M. Oreglia, "A Study of the Reactions $\psi' \to \gamma\gamma\psi$," PhD thesis, Stanford University, SLAC-R-0236, 1980.